

On the Influence of Channel Tortuosity on Electric Fields Generated by Lightning Return Strokes at Close Distance

Carlo Petrarca*, Simone Minucci, and Amedeo Andreotti

Abstract—In this paper the results of the estimated electric field associated with tortuous lightning paths at close distance (50 m to 500 m) are shown. Such results are compared with experimental data available in the literature and are illustrated along with a quantitative analysis of the field waveforms and their frequency spectra. The limits of the usual straight-vertical channel assumption and the influence of tortuosity at different azimuth and distances from the lightning channel base are also highlighted.

1. INTRODUCTION

A model for the estimation of electric and magnetic fields generated by lightning channels is extremely important [1–3]. Indeed, the computed fields can be used as input to models devoted to the calculation of induced voltages and currents, and their propagation, e.g., [4–8], can support the design of electrical protection system or help to size outdoor electrical components [9–11] and can be used to estimate the lightning protection level of existing structures [12]. Moreover, suitable computer models can help researchers in understanding the physics of lightning by deriving some typical physical parameters from measurements [13], such as the shape and rise of the return stroke current, its attenuation, distortion, and speed, and they can also improve the identification of the relationship of these parameters with electric field characteristics.

Many models have been proposed to study the cloud-to ground lightning and to calculate the fields. In particular, lightning return stroke models have been intensely studied, since the return stroke flashes are the most powerful known lightning processes [14, 15]. A significant limitation of most of these models is that the lightning channel is usually assumed to be straight and vertical although, actually, the path followed by a return stroke is tortuous [16]. Moreover, it is worth noticing that the lightning channel usually strikes the ground with a certain inclination with respect to the vertical, and its effects should not be neglected [17], since they can significantly affect both EM fields [18–20] and induced voltages [21–23]. Consequently, these simplified models are of great relevance but can miss some peculiar aspects, such as the fine structure and frequency content of the fields, or they can even underestimate their amplitude, both in natural and triggered lightning. It is therefore important to study the effects of channel tortuosity on the fields, by adopting a suitable geometrical structure of the path and a proper lightning return-stroke model.

A pioneering paper on modeling lightning electromagnetic fields produced by tortuous channels was presented by Le Vine and Meneghini [24], who used a piecewise linear model for a channel generated by interconnecting a series of segments automatically generated basing on assigned statistics. In order to predict the fields, the authors employed the Fraunhofer approximation, and consequently their results were limited to far-field computation (i.e., 100 km from the base of the channel). A significant contribution to overcome such a limitation was published in [25], where a closed-form solution for the

Received 27 January 2017, Accepted 27 March 2017, Scheduled 10 April 2017

* Corresponding author: Carlo Petrarca (petrarca@unina.it).

The authors are with the Department of Electrical Engineering and Information Technology, University of Naples Federico II, Naples 80125, Italy.

fields generated by a lightning channel with arbitrary location and slope was given, without introducing any approximation in the analytical field calculation. In [26], the results were also extended to a computer-generated tortuous channel, made of a series of arbitrarily oriented straight segments, treated individually.

A recent paper [27] detailed the influence of tortuous channels and, in particular, the contribution to distant electric fields of the return-stroke current speed of the lightning channel geometry and of its distance from the observer. Chia and Liew [28] obtained similar results on randomly generated tortuous lightning channels even though they limited their study only to one type of channel. Song et al. [29] also computed electromagnetic fields radiated from complex lightning channels. They showed that the tortuosity introduces frequency contents above 100 kHz and that the field intensity generated by a channel with branches is greater than the one generated by a single vertical channel. Their analysis was limited to very schematic shapes for the channel to reproduce tortuosity and also to a small number of observation points.

More recently, Meredith et al. [30] studied the effect of tortuosity by adopting an artificially generated path. Their finding was that tortuosity is only significant at relatively close distances and that the electromagnetic field produced by a tortuous channel becomes indistinguishable from that produced by a straight and vertical channel for distances greater than 1000 m. Their results were partial since they were extremely influenced by the shape of the generated channel, having a “zig-zag” symmetrical structure.

The effects produced by a “real” lightning channel (actually, only the x - z plane of a real channel was digitized from published photographs, while the y - z segments were artificially generated by computer) were then studied in [31]. Conversely, it was shown that, at close distances, tilt of the lower segments of the channel strongly affects the electric field amplitude (but not the waveshape) while only at larger distances, tortuosity produces jagged field waveforms.

The present paper has the aim to provide a further contribution to the understanding of the relationship between the lightning channel shape and the generated electric fields, by extending the analysis to close electric fields, which are fields generated at distances between 50 m and 500 m from the channel base. As in [31], the lightning channels have been digitized from real pictures [2]. The field waveforms and their frequency spectra have been computed and analyzed, and the results have been discussed and compared both to data obtained from numerical simulations on straight vertical lightning paths and to experimental data available in the literature, which are indeed very few. It is worth noticing that the model is general and able to calculate the fields at any point of the free space, but comparisons are limited to observation points at ground level where most of the experimental data are collected. Although the number and type of channels chosen for the simulations cannot be a representative set for a statistical description of the electric field waveforms, the results clearly show the contribution that a more detailed representation of the lightning channel geometry can give the characterization of the lightning electromagnetic environment.

In the following, Section 2 shows the lightning channels used for the simulations and provides the analytical solution for the electric field radiated by an arbitrarily oriented channel; Section 3 presents numerical results and discussions, and the conclusions are drawn in Section 4.

2. ELECTRIC FIELDS PRODUCED BY LIGHTNING CHANNELS

2.1. Tortuous Lightning Channels

The channels adopted for the simulations have been obtained by digitizing channel geometries of natural flashes recorded by Idone and Orville [32]; they are reproduced in Fig. 1.

Since in [32] only a 2D representation in the xz plane is given, the yz plane projection of the path is generated here by imposing two main constraints, on the mean absolute value [$\langle|\Delta\Omega|$] of the deviation angle from the average direction, and on the length L_b of each segment of the channel. In particular, for each channel, we have assumed $\langle|\Delta\Omega|$ = 17° and $5\text{ m} \leq L_b \leq 100\text{ m}$, according to data reported in [32]. Even though the number of constraints may appear higher than the degrees of freedom of each segment of the channel, it is worth stressing that the deviation angle is computed by using a Gaussian distribution whose median is $\langle|\Delta\Omega|$. Fig. 2 shows the obtained 3D paths of all the channels shown in Fig. 1.

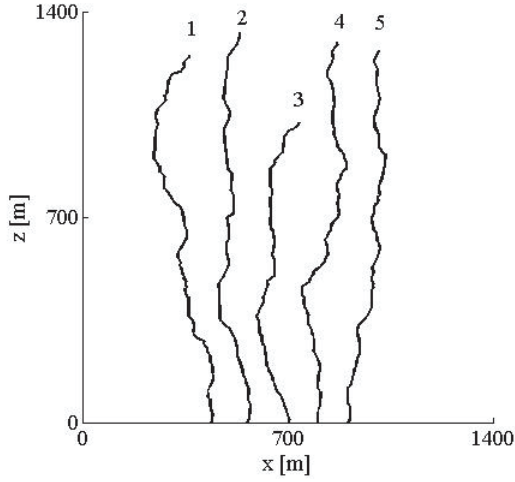


Figure 1. Lightning channels used for simulations (see Idone et al. [32]).

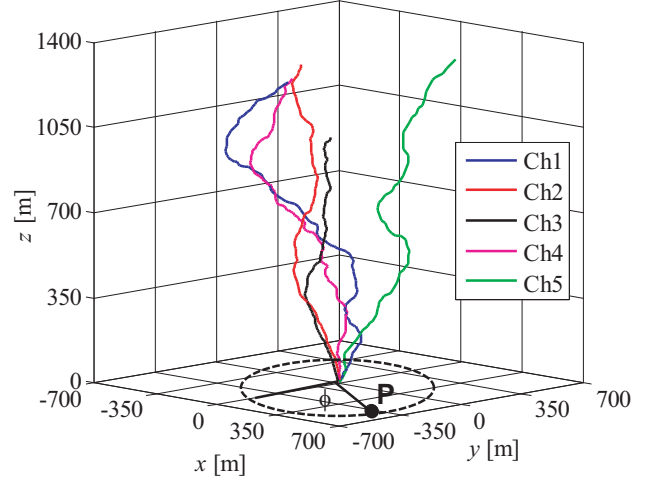


Figure 2. 3-D view of lightning channels. P is the observation point, ϕ is the azimuth angle.

2.2. Calculation of Electric Field

For EM fields calculation, the analytical approach adopted in [25] has been implemented, needing a simple analytical representation of the single discharge current, travelling an arbitrarily oriented channel \mathbf{C} as a function of time and space. In particular, it is possible to calculate the step response analytically by assuming that a unit step-function current travels along the channel:

$$i(z', t) = \left\{ u\left(t - \frac{z'}{v}\right) \left[u(z') - u(z' - h) \right] \right\} \quad (1)$$

where v is the return stroke front speed, and u is the Heaviside step function.

The overall effect of the tortuous channel can then be found by summing up the effects of the current $i(z', t)$ travelling through all its segments. Once the electric field due to a unit step current has been calculated, the field $y(t)$ associated with an arbitrary current waveform $i(t)$ can be obtained by convolution integration

$$y(t) = \int_0^t \frac{di(\tau)}{d\tau} s(t - \tau) d\tau \quad (2)$$

where $s(t)$ is the field component generated by a unit step current $u(t - \frac{z'}{v})$ travelling along \mathbf{C} , and $y(t)$ is the field component generated at the same point by the generic current $i(t)$.

By adopting a proper cylindrical reference system \mathfrak{R} (Fig. 3), with the z -axis coincident with the axis of the channel segment and the origin coincident with the starting point \mathbf{O} , the mathematical expression of the fields can be simplified since only r and z components of the electric field are present.

The generated electric field in the cylindrical reference system \mathfrak{R} at the observation point $P(r, \phi, z)$ assumes the formulation reported in Eq. (3), where c is the speed of light. The detailed calculations of the field can be found in [25] and [26].

$$\begin{cases} E_r = \frac{r \left[-tu \left(t - \frac{\sqrt{r^2+z^2}}{c} \right) \right]}{4\pi\epsilon_0 (\sqrt{r^2+z^2})^3} + \frac{r \left[-\left(t - \frac{l}{v}\right) u \left(t - \frac{l}{v} - \frac{\sqrt{r^2+(z-l)^2}}{c} \right) \right]}{4\pi\epsilon_0 (\sqrt{r^2+(z-l)^2})^3} + \int_0^l g(t) dz' \\ E_\phi = 0 \\ E_z = \frac{z \left[-tu \left(t - \frac{\sqrt{r^2+z^2}}{c} \right) \right]}{4\pi\epsilon_0 (\sqrt{r^2+z^2})^3} + \frac{(z-l) \left[\left(t - \frac{l}{v}\right) u \left(t - \frac{l}{v} - \frac{\sqrt{r^2+(z-l)^2}}{c} \right) \right]}{4\pi\epsilon_0 (\sqrt{r^2+(z-l)^2})^3} + \int_0^l p(t) dz' \end{cases} \quad (3)$$

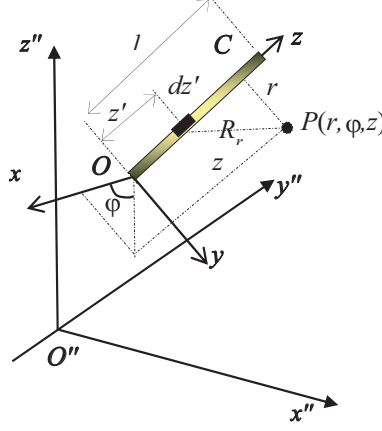


Figure 3. Generic discharge channel **C** and main geometrical parameters.

where the integrals $\int_0^l g(t) dz'$ and $\int_0^l p(t) dz'$ have the following values:

$$\int_0^l g(t) dz' = \begin{cases} 0 & \text{if } z_0(t) < 0 \\ \frac{1}{4\pi\epsilon_0 v} \left[\frac{\sin(\varphi_2) - \sin(\varphi_1)}{r} + \frac{r}{cR_0^2 \left| -\frac{1}{v} - \frac{(z_0(t)-z)}{cR_0} \right|} \right] & \text{if } 0 \leq z_0(t) \leq l \\ \frac{1}{4\pi\epsilon_0 v} \left[\frac{\sin(\arctg(\frac{l-z}{r})) - \sin(\arctg(-\frac{z}{r}))}{r} \right] & \text{if } z_0(t) > l \end{cases} \quad (4)$$

$$\int_0^l p(t) dz' = \begin{cases} 0 & \text{if } z_0(t) < 0 \\ \frac{1}{4\pi\epsilon_0 v} \left[\frac{\cos(\varphi_2) - \cos(\varphi_1)}{r} + \frac{(z - z_0(t))}{cR_0^2 \left| -\frac{1}{v} - \frac{(z_0(t)-z)}{cR_0} \right|} \right] & \text{if } 0 \leq z_0(t) \leq l \\ \frac{1}{4\pi\epsilon_0 v} \left[\frac{\cos(\arctg(\frac{l-z}{r})) - \cos(\arctg(-\frac{z}{r}))}{r} \right] & \text{if } z_0(t) > l \end{cases} \quad (5)$$

in which

$$z_0(t) = \frac{\frac{t}{v} - \frac{z}{c^2} - \sqrt{\left(\frac{t}{v} - \frac{z}{c^2}\right)^2 - \left(\frac{1}{v^2} - \frac{1}{c^2}\right) \left(t^2 - \frac{r^2}{c^2} - \frac{z^2}{c^2}\right)}}{\left(\frac{1}{v^2} - \frac{1}{c^2}\right)} \quad (6)$$

and

$$\begin{cases} \varphi_1 = \arctg\left(-\frac{z}{r}\right) \\ \varphi_2 = \arctg\left(\frac{z_0(t)-z}{r}\right) \\ R_0 = \sqrt{r^2 + (z - z_0(t))^2} \end{cases} \quad (7)$$

Since the electric field has to be calculated in the presence of a soil-air interface, the image principle has been adopted [33], turning the analysis in two different media into an equivalent analysis carried out in one homogeneous medium, by properly placing a set of sources into the whole free space. Their magnitude is calculated in such a way to keep the same interface conditions on the separation surface between the two media. Thanks to the uniqueness of the solution of Maxwell's equation with prescribed boundary conditions, the superposition of the two “image solutions” gives the total electric field as in the real geometry, in which the soil-air interface is taken into account.

The ground is modelled as a perfectly conducting plane (i.e., its conductivity is infinite) and the contribution of the image sources has been obtained in the same way, by adopting a cylindrical coordinate system with the z -axis coincident with the axis of the image channel.

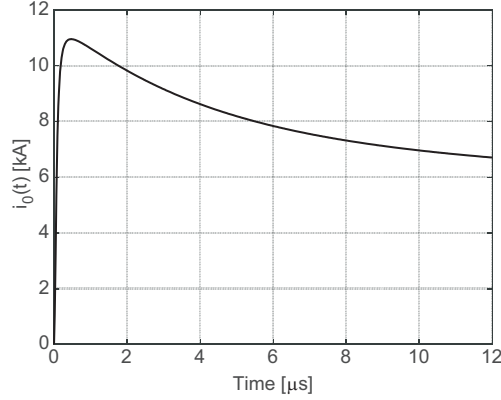


Figure 4. Channel base return stroke current adopted in the simulations.

Concerning the analytical expression of the channel base current, the sum of a Heidler function [34] and a double exponential function has been used in Eq. (8) because it is well suited for successive return strokes. Therefore, it can be used as source at the channel base for the propagation along the photographed channels of Fig. 1.

$$i(0, t) = \frac{I_{01}}{\eta} \frac{\left(\frac{t}{\tau_1}\right)^n}{1 + \left(\frac{t}{\tau_1}\right)^n} e^{-\frac{t}{\tau_2}} + I_{02} \left(e^{-\frac{t}{\tau_3}} - e^{-\frac{t}{\tau_4}} \right) \quad (8)$$

If the values proposed in [35] are adopted ($\tau_1 = 0.072 \mu\text{s}$, $\tau_2 = 5.0 \mu\text{s}$, $\tau_3 = 100 \mu\text{s}$, $\tau_4 = 6.0 \mu\text{s}$, $I_{01} = 9.9 \text{ kA}$, $I_{02} = 7.5 \text{ kA}$, $\eta = 0.845$ and $n = 2$), we get the waveform shown in Fig. 4.

The current is assumed to propagate at constant speed $v = 120 \text{ m}/\mu\text{s}$ ($\beta = \frac{v}{c} = 0.4$) and to decay with the height according to the Modified Transmission Line Linear (MTLL) model [36], which is appropriate for electric field waveforms at close distances. A linear current decay along the channel is considered, from a maximum value at the channel base to zero at the channel top. The parameter H is 7.5 km.

3. RESULTS AND DISCUSSION

The electric field has been calculated at the ground surface ($z = 0$) at different distances d (50 m, 150 m, 250 m and 500 m) from the channel base and at different azimuth values ϕ . In particular, for each distance d , 24 observation points P were selected, starting from $\phi = 0^\circ$ up to $\phi = 360^\circ$, in steps of $\Delta\phi = 15^\circ$ (see Fig. 2). In this way, it is possible to show the dependence of the fields on the relative position between the channel and the observation point and to focus on the differences with the fields calculated by adopting a simple vertical channel model, which are ϕ independent.

Before carrying out the analysis of the fields, it should be considered that experimental data for electric fields generated at close distance by downward natural lightning discharges to ground are few and limited. In fact, for evident difficulties, most of the measurements are taken during triggered lightning, formed by an upward-extending leader, different from natural lightning. For this reason, we remark that, in what follows, experimental data should only be considered as a valuable help in interpreting the results from simulation but cannot be used as a benchmark for testing the validity of the model.

3.1. Electric Field $E(t)$

Electric field waveshapes from return strokes measured at 1 to 200 km are presented in [37] and classified in [38]. Electric and magnetic field waveshapes generated by leader and return stroke, measured at close distance, can be found in [39–41]. A typical electric field waveform shows:

- (i) an initial “slow front” lasting from five up to ten microseconds;

- (ii) a successive sharp increase in few microseconds;
- (iii) the presence of a “first peak” (not always visible at very close distances);
- (iv) a characteristic flattening, due to the main contribution given by the electrostatic component.

Sometimes the waveforms exhibit small “humps”, whose origin is uncertain, but that can be probably due to charge motion in channels with major bends (Fig. 5).

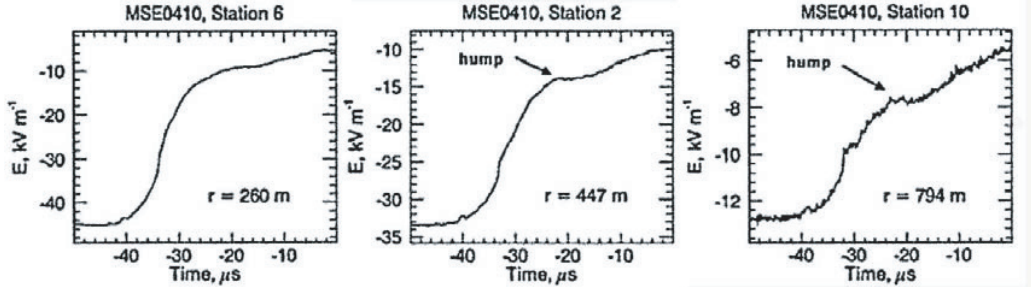


Figure 5. Measured E -field waveforms. Adapted from Jerauld et al. [39].

The electric field waveforms calculated from the simulations on tortuous channels, as shown in Fig. 6, are able to reproduce these typical characteristics. As an example, in Fig. 6 the time evolution of the vertical electric field calculated at ground, at four different distances (50 m, 150 m, 250 m and 500 m) and four different observation points ($\phi = 90^\circ$, $\phi = 135^\circ$, $\phi = 165^\circ$, $\phi = 270^\circ$) are illustrated, in the case of lightning channel n.1.

The field evolution presents both the sharp increase and “humps”, but not the “slow front” characteristic; this is probably due to the presence of an upward connecting leader [38] which, as discussed above, is not accounted in the present model, but is typical for triggered channels.

In Fig. 6, the electric field waveform generated by a vertical lightning path is also plotted as a benchmark, in order to show effects of the channel geometry in clear detail. At very close distances (up to 150 m), the effect of channel tortuosity is negligible; indeed, the electric field waveforms show a regular shape, with no presence of a “first peak” and no jaggedness. Such a behavior can be explained by considering the contributions to the E -field of each segment composing the channel: the lower sections of the lightning path (i.e., those near the ground) dwarf the effects of the upper sections. A slight effect of tortuosity is given by small “humps” visible in Fig. 6(b) at position $\phi = (135^\circ, 270^\circ)$.

Moreover, the effect of the channel inclination (mainly of the lower segments of the channel) is considerable, because the electric field is now strongly dependent on the observation point and can be significantly different from the field calculated in the same point and produced by a vertical channel. As an example, if in Fig. 6(a) we calculate the electric field amplitude E_p at $t = 2 \mu\text{s}$ after the stroke initiation and compare it to the value obtained for a vertical channel ($E_{pv} = 25.6 \text{ kV m}^{-1}$), we find that such a value is much higher ($E_p = 60.4 \text{ kV m}^{-1}$) at $\phi = 90^\circ$ and sensibly lower ($E_p = 14.6 \text{ kV m}^{-1}$) at the opposite observation point $\phi = 270^\circ$. Such an aspect puts in evidence a great limitation of the straight vertical channel model; it will be discussed in detail in subsection 3.2 of the present section.

When looking at distances higher than 250 m, the fine structure of the fields due to channel tortuosity starts to appear, and the small “humps” are much more pronounced (see Figs. 6(c) and 6(d)). In fact, the upper segments of the lightning channel are no longer “masked” by the lower sections and give their significant contribution to the electric field.

At these distances, the tortuous model is also able to reproduce another interesting feature of close electric fields, namely a very fast transition in a time interval of a few hundreds of nanoseconds towards a “first peak”, followed by a slower increase of the field [38]. The first peak is due to the field radiation component, it is almost independent of the observation point and can be now more easily identified, if compared to closer waveforms. This aspect cannot be considered in the straight vertical channel model.

The calculation of the electric fields generated by all the channels represented in Fig. 1 shows that all the corresponding waveforms exhibit similar behaviors, although the channels can be very different from each other. For example, it is possible to compare the fields generated by channel n.1 (shown in Fig. 6) and those generated by channel n.2 (shown in Fig. 7).

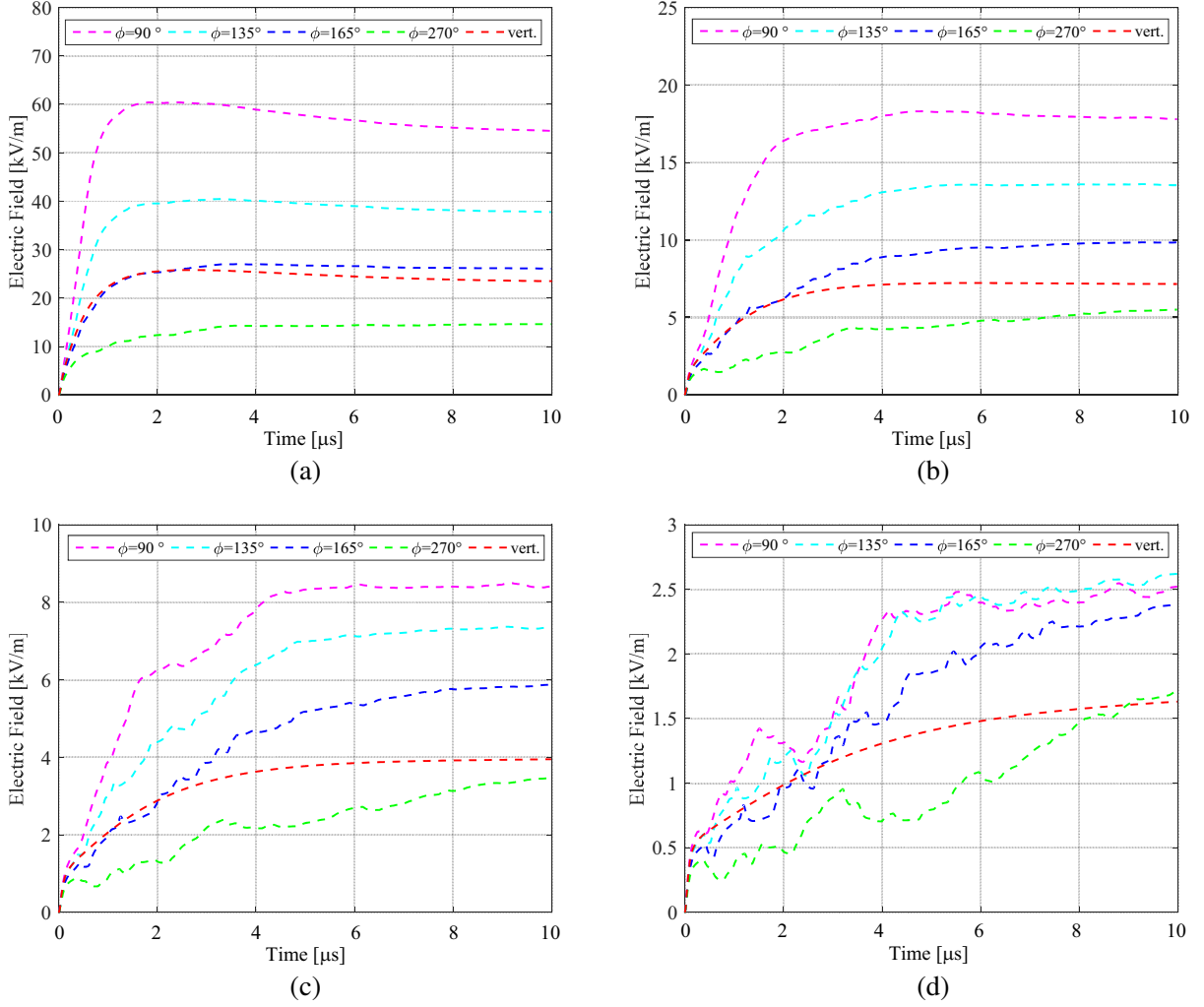


Figure 6. Electrical field $E(t)$ at (a) $d = 50$ m, (b) $d = 150$ m, (c) $d = 250$ m and (d) $d = 500$ m as a function of the azimuth angle ϕ (channel n.1). The red line corresponds to $E(t)$ generated by a vertical channel.

Also in this case it is possible to observe that there is always an observation point P_M ($\phi = 300^\circ$ in Fig. 7(a)) where the highest value of the electric field is reached and a point P_m , on the opposite side ($\phi = 120^\circ$ in Fig. 7(a)), with the lowest value at close distances. Moreover, the effects of tortuosity and “humps” are evident at distances above 250 m, where the presence of the first peak in the electric field can also be noticed.

3.2. Effects of Channel Inclination

The effects of the inclination of the lower segments of the channel can be described by introducing the parameter $DE_\phi\%$, which describes the “distance” between the time evolution of the electric field $E_{p\phi}(t)$ (produced by a tortuous lightning path and calculated at azimuth ϕ) and the electric field $E_{pv}(t)$ (generated by a vertical channel and calculated in the same observation point).

In order to evaluate the parameter $DE_\phi\%$, we have to consider the two time-series $E_{p\phi}(k)$ and $E_{pv}(k)$, calculated in a fixed time interval T_s , where $k = 1, 2, \dots, N_s$, N_s being the number of samples. The parameter is defined by the following Equation (9):

$$DE_\phi\% = \frac{1}{N_s} \sum_{k=1}^{N_s} \left(\left| \frac{E_{p\phi}(k) - E_{pv}(k)}{E_{pv}(k)} \right| \right) \cdot 100 \tag{9}$$

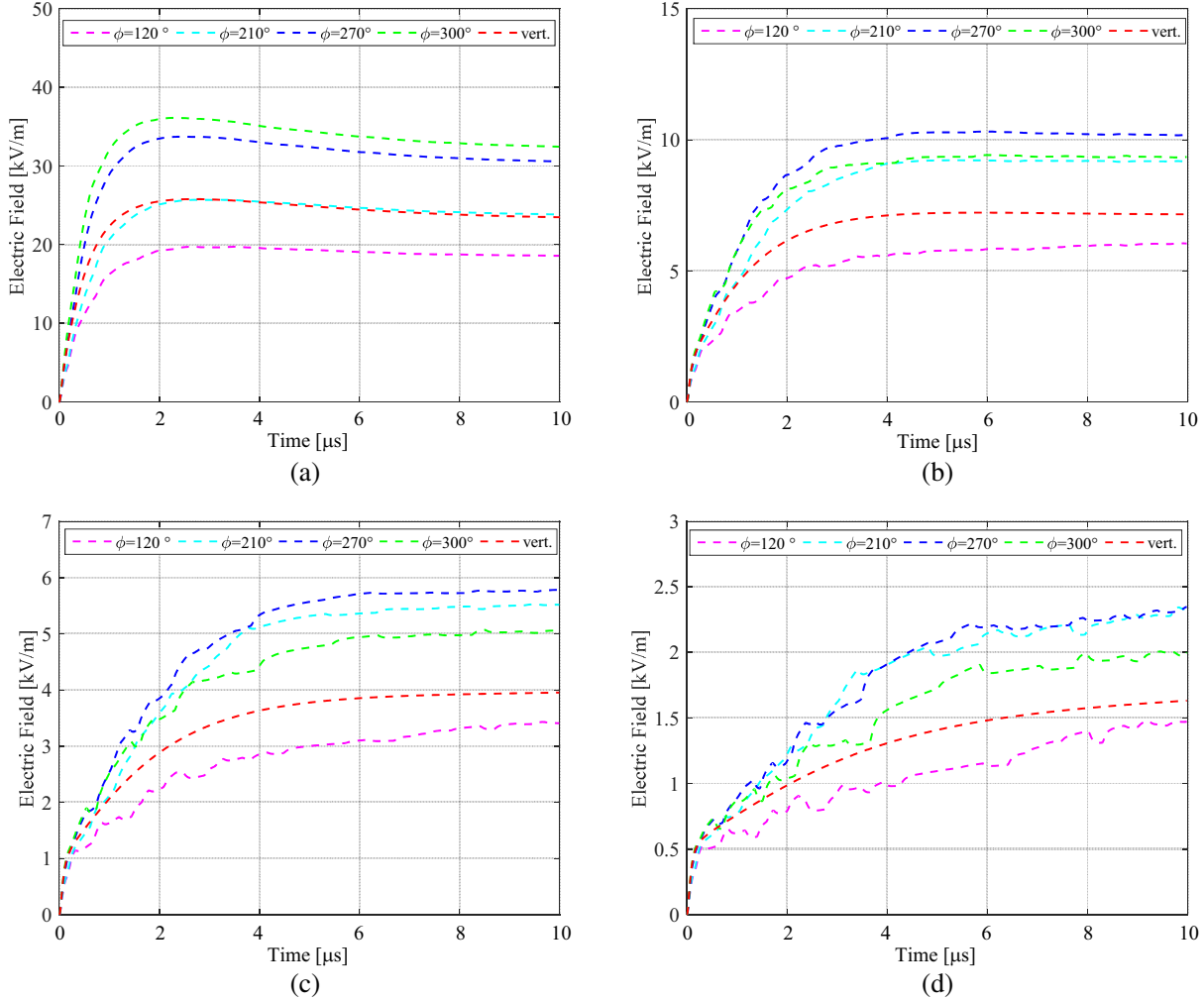


Figure 7. Electrical field $E(t)$ at (a) $d = 50$ m, (b) $d = 150$ m, (c) $d = 250$ m and (d) $d = 500$ m as a function of the azimuth angle ϕ (channel n.2). The red line corresponds to $E(t)$ generated by a vertical channel.

If the fields are equal, then $DE_\phi\% = 0$; otherwise, $DE_\phi\%$ increases as the difference in the calculated fields is greater.

Figure 8 shows $DE_\phi\%$ calculated in the time interval $T_s = 10 \mu\text{s}$ as a function of the azimuth angle ϕ at various distances, for channels 1 to 5. From the figure we can infer that the electric field can be sensibly different from the field produced by a straight vertical channel, depending on the observation point and on the shape of the lightning path. For instance, at $d = 50$ m (Fig. 8(a)), for channel 1 we find a maximum ($DE_{\phi_{\max}}\% = 130\%$) at $\phi = 90^\circ$ and a minimum ($DE_{\phi_{\min}}\% = 7\%$) at $\phi = 0^\circ$ and $\phi = 165^\circ$; for channel 5, the maximum ($DE_{\phi_{\max}}\% = 116\%$) is calculated at $\phi = 75^\circ$ while the minimum $DE_{\phi_{\min}}\% = 2.7\%$ can be found, again, at $\phi = 0^\circ$ and $\phi = 165^\circ$. Less pronounced are the maxima calculated for channel 2 and channel 3 ($DE_{\phi_{\max}}\% = 38\%$ and $DE_{\phi_{\max}} = 41\%$, respectively) while only for channel 4, $DE_\phi\%$ is very small and almost independent of ϕ . In the latter case the field amplitude is almost equal to that generated by a lightning current flowing along a vertical path.

Such behavior can be explained by carefully observing Fig. 9. In this figure we have shown: i) on the left side the relative position of the observer with respect to the lightning channels (channel 1, pictured in black, and channel 4, depicted in magenta); ii) on the right side the time evolution of the electric field calculated in the position of the observer (50 m) and produced by the same current flowing in the aforementioned channels and in the vertical one.

At viewpoint $\phi = 0^\circ$ (Fig. 9(a)) both channels 1 and 4 appear nearly vertical to the observer: in

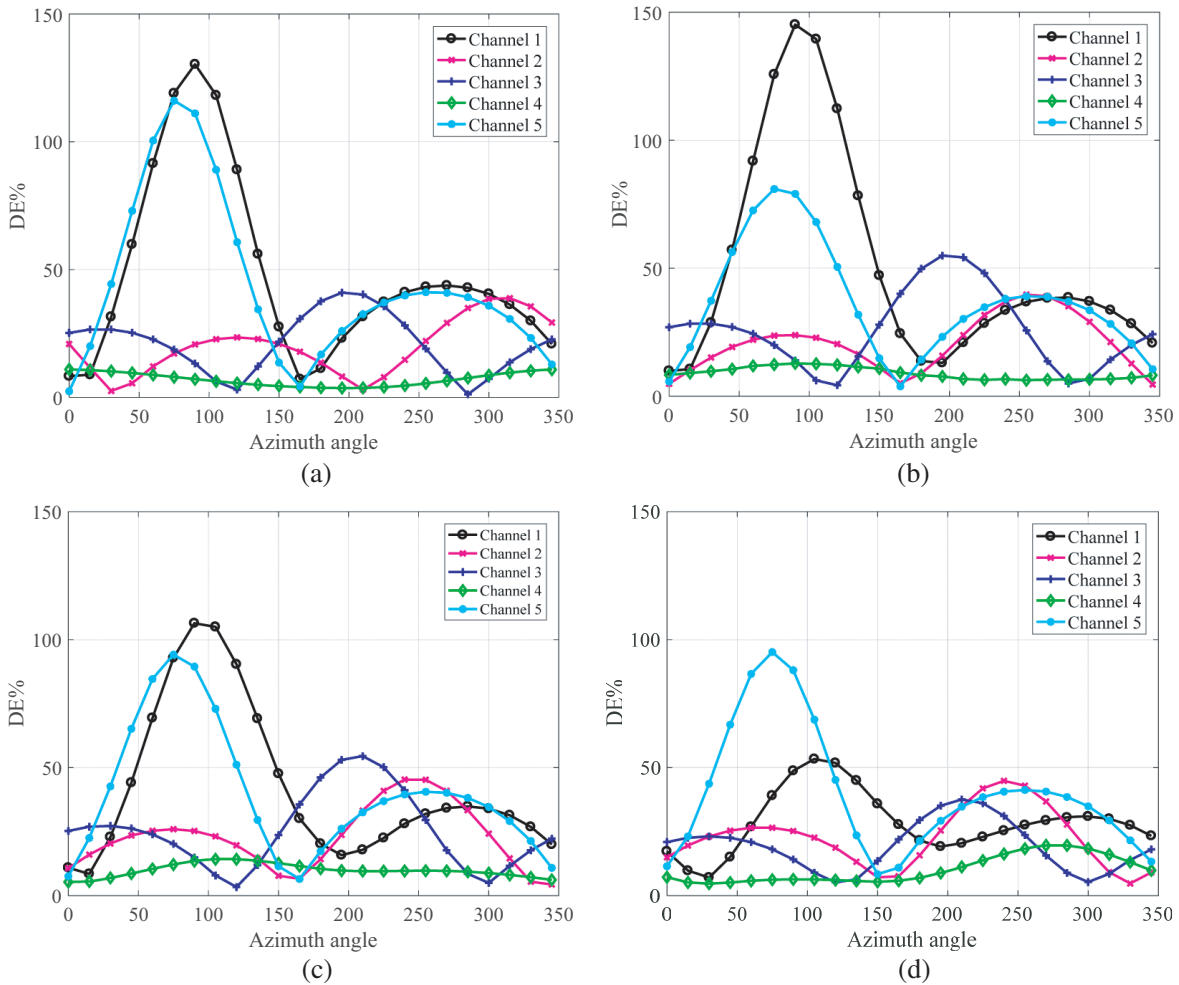


Figure 8. Parameter $DE_\phi\%$ as a function of azimuth angle at various distances, (a) $d = 50$ m, (b) $d = 150$ m, (c) $d = 250$ m and (d) $d = 500$ m.

such position $DE_\phi\%$ is very low, and the electrical field amplitude is very similar to that calculated for a vertical lightning path, as confirmed by the waveforms shown in Fig. 9(e). The electric field waveforms show analogous behavior (Fig. 9(g)) if being calculated at viewpoint $\phi = 165^\circ$ (Fig. 9(c)); in fact in that position the shape of the channels still resembles that of a vertical path.

At position $\phi = 90^\circ$ (Fig. 9(b)), channel 4 is still “seen” as vertical by the observer, while channel 1 is extremely inclined towards it. The respective electric fields, as depicted in Fig. 9(f), are significantly different: i) the field produced by channel 4 is almost equal to the field produced by the vertical channel, and $DE_\phi\%$ in that position is very low ($DE_\phi\% = 7\%$); ii) the field produced by channel 1 is sensibly higher and $DE_\phi\% \sim 130\%$. In particular at time instant $t = 2 \mu\text{s}$, the electric field amplitude due to a vertical channel is $E = 25.5 \text{ kV/m}$, while the field produced by channel 1 is $E = 60 \text{ kV/m}$, i.e., 235% higher. The limits of the vertical channel model are in this case clearly pointed out.

In Fig. 9(d), corresponding to the viewpoint $\phi = 270^\circ$, the lightning channel 1 moves away from the observer, and the resulting electric field is again different from the field produced by a vertical path ($DE_\phi\% = 40\%$), but in this case, its amplitude is much lower ($E = 12.3 \text{ kV/m}$ at $t = 2 \mu\text{s}$) than the field computed with the vertical channel ($E = 25.5 \text{ kV/m}$). Again, the proposed model shows the limitations of using a simplified cylindrically symmetric electric field distribution.

Another interesting feature can be obtained by analyzing the electric field produced by channel 1 and channel 5 at a distance $d = 150$ m and $d = 500$ m and calculated at the viewpoint $\phi = 90^\circ$. From Figs. 8(b) and 8(d), we derive that the index $DE_\phi\%$ decreases with distance for channel 1 (from 145% at $d = 150$ m to 49% at $d = 500$ m) while it increases for channel 5 (from 80% at $d = 150$ m to 95%

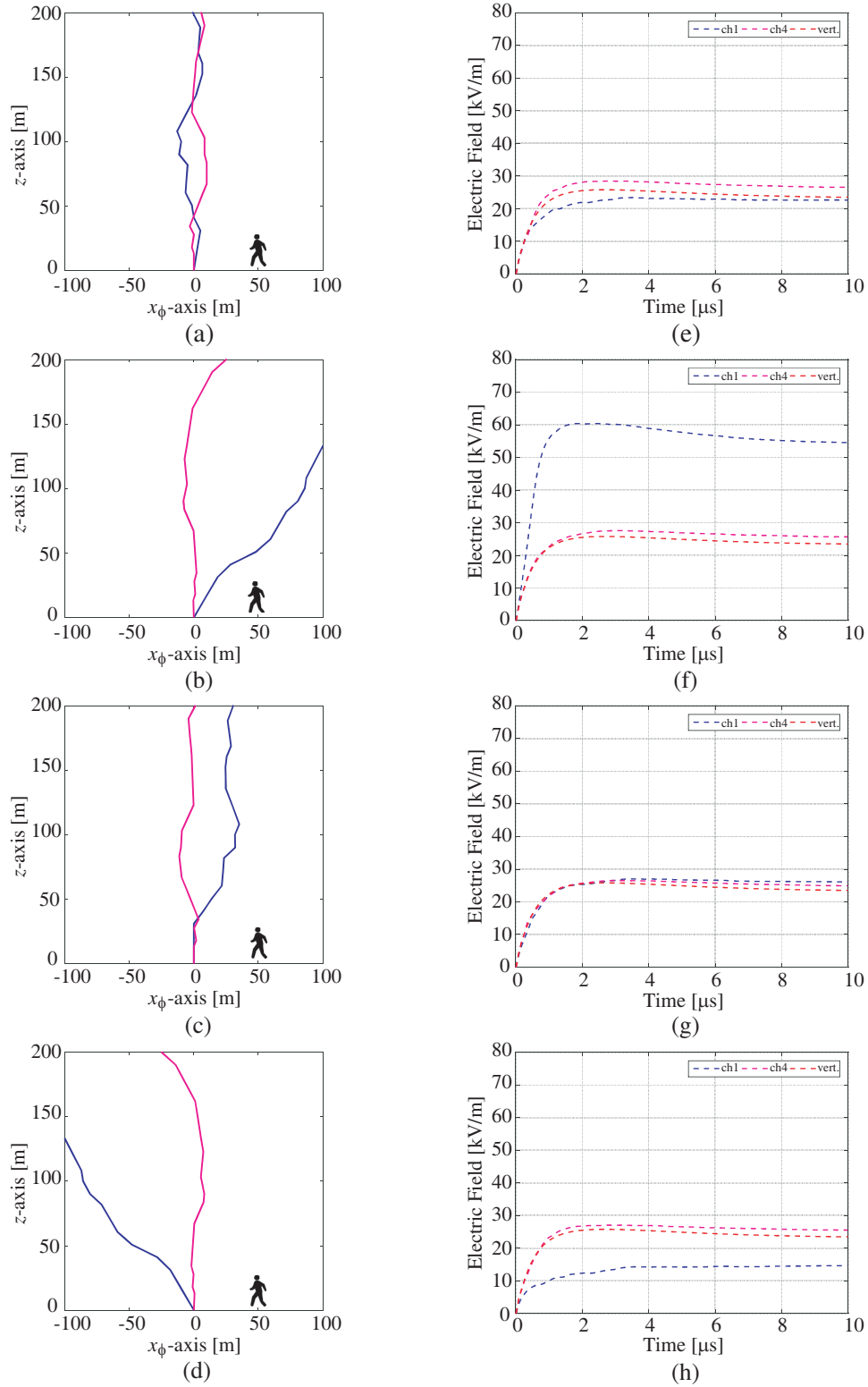


Figure 9. Channel 1 (blue) and channel 4 (magenta) seen from different observation points at $d = 50$ m. (a) $\phi = 0^\circ$, (b) $\phi = 90^\circ$, (c) $\phi = 165^\circ$ and (d) $\phi = 270^\circ$ and (e), (f), (g), (h) corresponding time evolution of the electric field.

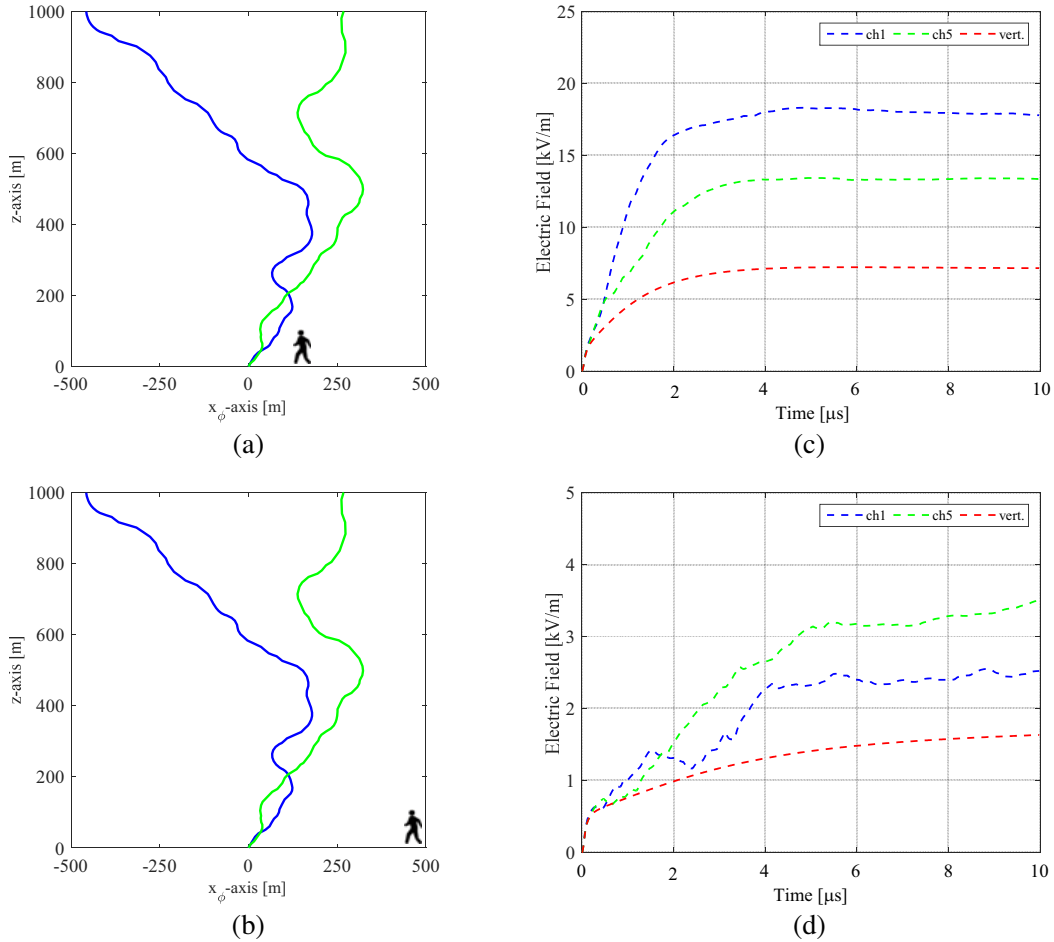


Figure 10. Channel 1 (blue) and channel 5 (green) seen observation point $\phi = 90^\circ$ at (a) $d = 150$ m, (b) $d = 500$ m and (c), (d) corresponding time evolution of the electric field.

at $d = 500$ m). The explanation of such a behavior can be found again in the relative position of the observer with respect to the lightning path. At close distance ($d = 150$ m) channel 1 is more inclined than channel 5 with respect to the observer, and the produced electric field differs from that of a vertical one much more than the latter (Fig. 10(c)). At $d = 500$ m, the inclination of lower channel segments has a minor influence, and the waveform of the electric field depends on the shape of the entire lightning path, as confirmed by Figs. 10(b) and 10(d).

3.3. Electric Field Spectra

The knowledge of the electric field spectra can be of great importance to characterize the lightning phenomena, since it can be a very useful tool both for scientific investigations on lightning discharge physics and for engineering assessment threat on electronic devices.

Lightning spectra have been generally obtained by two main techniques: using narrow-band receivers, which measure the energy radiated at the tuning frequency or recording the electric field waveform with wide bandwidth instruments and then applying the Fourier transformation [42, 43].

Experimental data generally refer to distant fields (up to some km) and show that return strokes are the strongest source of radio-frequency radiation in the interval from [0.2–20] MHz. Within this interval, the spectra are quite similar for various lightning events, and their amplitude mainly decreases as the inverse of frequency (f^{-1}) [1, 42–44].

Figure 11 shows the spectra obtained as the average amplitude for 15 cloud-to-ground discharges observed in 2002 in Tibet area [42].

The results of the simulations for channel 1 are shown in Fig. 12. The electric field spectra at close distance (from $d = 50$ m to $d = 250$ m) in the range $[0.7 \div 70]$ MHz are similar to that of a vertical channel; moreover, they do not depend on azimuth angles, and their amplitude tends to decrease roughly as f^{-1} .

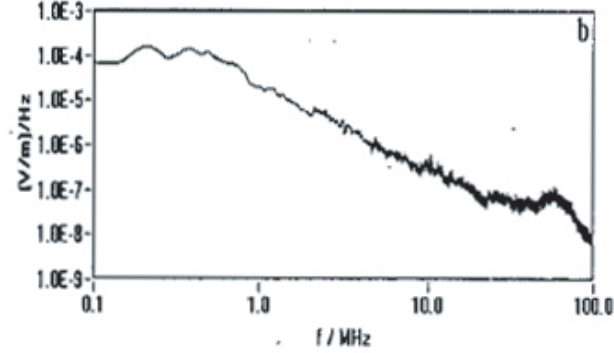


Figure 11. Measured E -field spectra at 10 km. Adapted from Chen et al. [42].

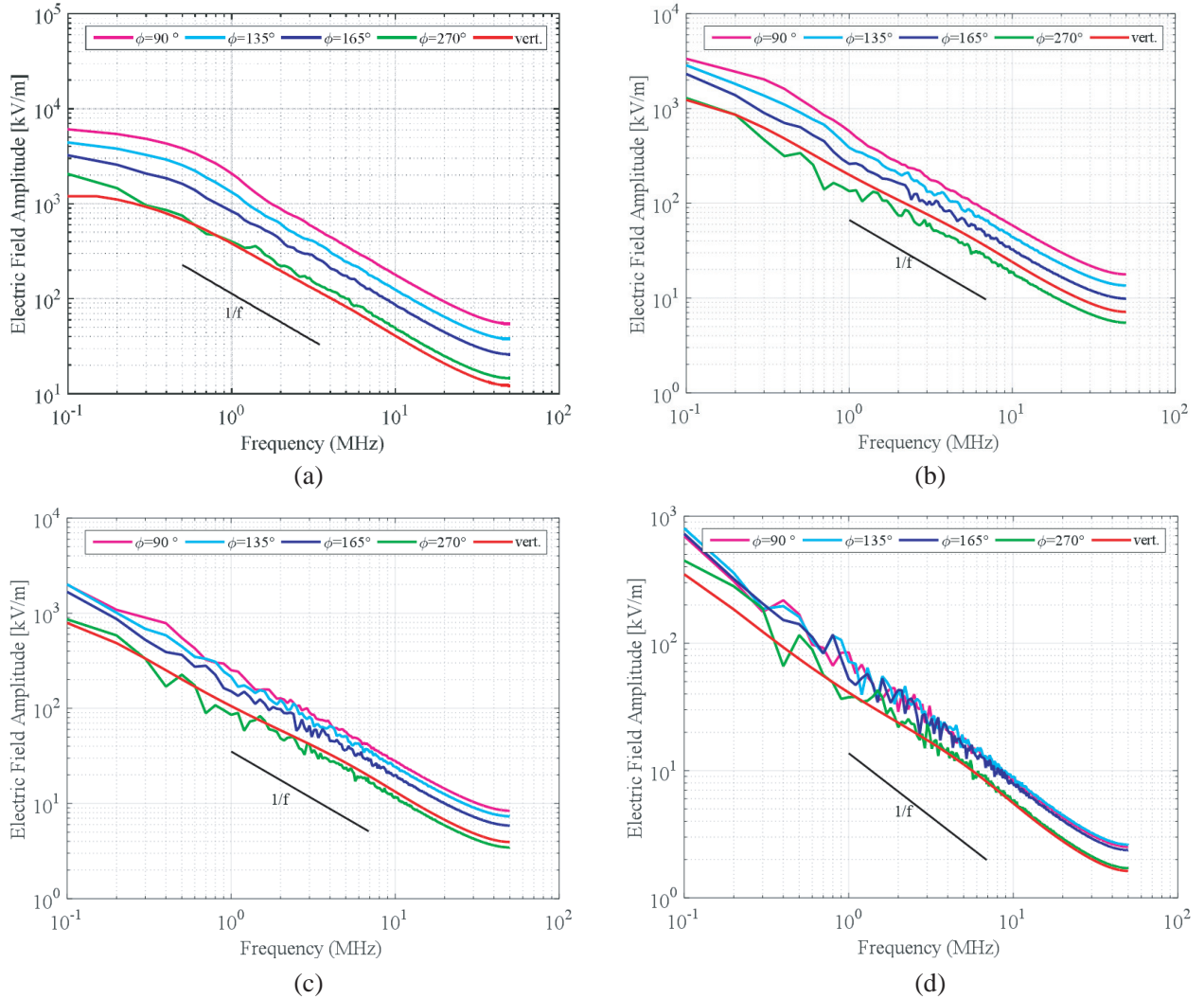


Figure 12. Electrical field spectra at (a) $d = 50$ m, (b) $d = 150$ m, (c) $d = 250$ m, and (d) $d = 500$ m as a function of azimuth angle (Channel n.1). The red line corresponds to the spectra of a vertical channel.

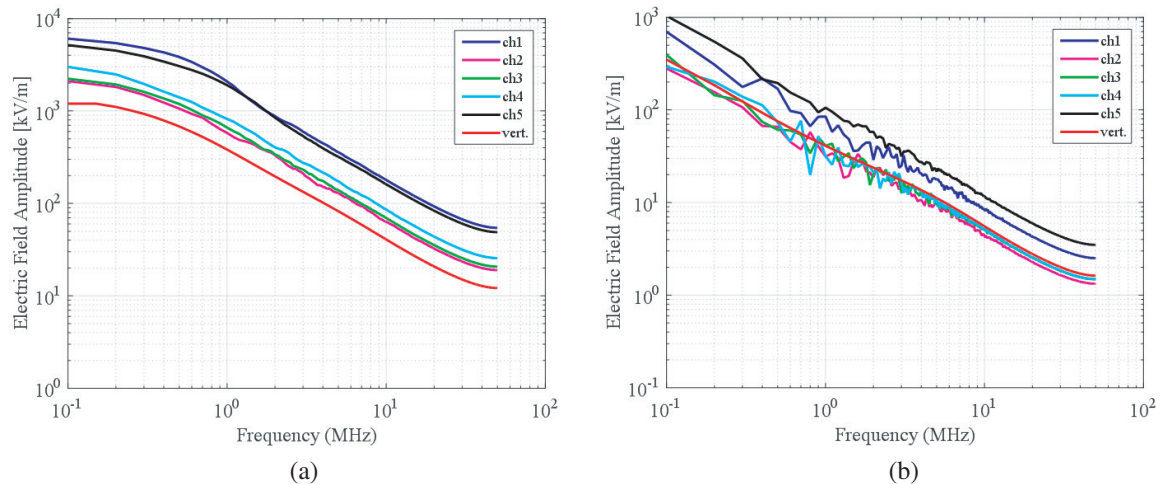


Figure 13. Electrical field spectra by channels 1 to 5 at azimuth angle $\varphi = 90^\circ$ at (a) $d = 50$ m, (b) $d = 500$ m. The red line corresponds to the electrical field spectrum of a vertical channel.

At greater distance, the effect of tortuosity introduces an increase in the frequency content above 200 kHz. In fact, each kink generates a change in the direction of propagation of the current which creates a rapid change in the electric field. With respect to the spectra produced by a vertical channel, the main changes in the amplitude generally occur at frequencies in the range around $300 \text{ kHz} \div 3 \text{ MHz}$, irrespectively of the azimuth angle.

The results are confirmed by Fig. 13 where the frequency spectra for all the 5 lightning channels, calculated at azimuth position $\phi = 90^\circ$ and at distance $d = 50$ m and $d = 500$ m are plotted. At close distance the spectra are similar to that of a vertical channel, although scaled, whilst farther from the channel base changes in the frequency content are observed in the range $300 \text{ kHz} - 3 \text{ MHz}$.

4. CONCLUSIONS

Channel tortuosity can significantly affect the electric field generated by cloud-to-ground lightning. At close distance, the field amplitude mainly depends on the inclination of the bottom segments of the channel and on the relative position of the observer. Fields can be even doubled if being compared to the field produced by a vertical channel. At longer distances the effect of the overall tortuosity can be better seen, because of the effect of a longer portion of the lightning channel which is affected by the return stroke current. Frequency spectrum is dependent on tortuosity, and differences with a vertical channel can be found in the range $300 \text{ kHz} \div 3 \text{ MHz}$. These considerations point out the limits of the evaluation of electric fields based on a simplified model in which the lightning path is considered vertical. Such aspects should be considered in computer models used for the estimation of the fields generated by lightning.

REFERENCES

1. Uman, M. A. and V. A. Rakov, *Lightning Physics and Effects*, Cambridge University Press, 2007.
2. Uman, M. A., *The Art and Science of Lightning Protection*, Cambridge University Press, New York, 2008.
3. Cooray, V., (editor), *Lightning Electromagnetics, IET Power and Energy Series 62*, 2012.
4. Rachidi, F., C. A. Nucci, and M. Ianoz, "Transient analysis of multiconductor lines above a lossy ground," *IEEE Trans. Power Delivery*, Vol. 14, No. 1, 294–302, Jan. 1999.
5. Diendorfer, G., "Induced voltage on an overhead line due to nearby lightning," *IEEE Trans. on Electromagnetic Compatibility*, Vol. 32, No. 4, 292–299, Nov. 1990.
6. Høidalen, H. K., J. Slebtak, and T. Henriksen, "Ground effects on induced voltages from nearby lightning," *IEEE Trans. on Electromagnetic Compatibility*, Vol. 32, No. 4, 292–299, Nov. 1990.

7. Andreotti, A. P. and V. A. Rakov, "An analytical approach to calculation of lightning induced voltages on overhead lines in case of lossy ground — Part I: Model development," *IEEE Trans. Power Delivery*, Vol. 28, No. 2, 1213–1223, Nov. 2013.
8. Andreotti, A. P. and V. A. Rakov, "an analytical approach to calculation of lightning induced voltages on overhead lines in case of lossy ground — Part II: Comparison with other models," *IEEE Trans. Power Delivery*, Vol. 28, No. 2, 1224–1230, Nov. 2013.
9. Borghetti, A., S. Morched, F. Napolitano, C. A. Nucci, and M. Paolone, "Lightning-induced overvoltages transferred through distribution power transformers," *IEEE Trans. Power Delivery*, Vol. 24, No. 1, 360–372, Jan. 2009.
10. Tesche, F. M., A. W. Kälin, B. Brändli, B. Reusser, M. Ianoz, D. Tabar, and P. Zwiackner, "Estimates of lightning-induced voltage stresses with buried shielded conduits," *IEEE Trans. on Electromagnetic Compatibility*, Vol. 40, 492–504, 1998.
11. Petrache, E., F. Rachidi, M. Paolone, C. A. Nucci, V. A. Rakov, and M. A. Uman, "Lightning induced disturbances in buried cables — Part I: Theory," *IEEE Trans. on Electromagnetic Compatibility*, Vol. 47, No. 3, 498–508, 2005.
12. IEEE Guide for Improving the Lightning Performance of Electric Power Overhead Distribution Lines, IEEE Standard 1410, 2010.
13. Cummins, K. L., "Lightning information for use in power systems analysis: How much more do we need to know?," *Transmission and Distribution Conference and Exhibition 2002: Asia Pacific, IEEE/PES*, Vol. 1, 529–533, Yokohama, Japan, Oct. 2002.
14. Rakov, V. A. and M. A. Uman, "Review and evaluation lightning return stroke models including some aspects of their application," *IEEE Trans. on Electromagnetic Compatibility*, Vol. 40, No. 4, 403–426, 1998.
15. Rakov, V. A. and F. Rachidi, "Overview of recent progress in lightning research and lightning protection," *IEEE Trans. on Electromagnetic Compatibility*, Vol. 51, No. 3, 428–442, 2009.
16. Uman, M. A., *The Lightning Discharge*, Academic Press, San Diego, CA, 1987.
17. Uman, M., J. Schoene, V. Rakov, K. J. Rambo, and G. H. Schnetzer, "Correlated time derivatives of current, electric field intensity and magnetic flux density for triggered lightning at 15 m," *Journal of Geophysical Research*, Vol. 107, 4160–4172, 2002.
18. Izadi, M., M. Z. A. A. Kadir, and C. Gomes, "Evaluation of electromagnetic fields associated with inclined lightning channel using second order FDTD-hybrid methods," *Progress In Electromagnetics Research*, Vol. 117, 209–236, 2011.
19. Gomes, C., V. Cooray, and M. Z. A. Ab Kadir, "Vertical electric fields and field change parameters due to partly inclined lightning leader channels," *Progress In Electromagnetics Research*, Vol. 135, 55–80, 2013.
20. Amarasinghe, D., U. Sonnadara, M. Berg, and V. Cooray, "Channel tortuosity of long laboratory sparks," *Journal of Electostatics*, Vol. 65, No. 8, 521–526, 2007.
21. Andreotti, A., U. De Martinis, C. Petrarca, V. A. Rakov, and L. Verolino, "Lightning electromagnetic fields and induced voltages: Influence of channel tortuosity," *30th URSI General Assembly and Scientific Symposium, URSIGASS*, paper 6050702, Turkey, 2011.
22. Andreotti, A., C. Petrarca, V. A. Rakov, and L. Verolino, "Calculation of voltages induced on overhead conductors by nonvertical lightning channels," *IEEE Trans. on Electromagnetic Compatibility*, Vol. 54, No. 4, 860–870, Jan. 2012.
23. Andreotti, A., C. Petrarca, and A. Pierno, "On the effects of channel tortuosity in lightning-induced voltages assessment," *IEEE Trans. on Electromagnetic Compatibility*, Vol. 57, No. 5, 1096–1102, Oct. 2015.
24. Le Vine, M. and R. Meneghini, "Simulation of radiation from lightning return strokes: The effects of tortuosity," *Radio Sci.*, Vol. 13, No. 5, 801–809, Sep./Oct. 1978.
25. Lupò, G., C. Petrarca, V. Tucci, and M. Vitelli, "EM fields generated by lightning channels with arbitrary location and slope," *IEEE Trans. on Electromagnetic Compatibility*, Vol. 42, No. 1, 39–53, Feb. 2000.

26. Lupò, G., C. Petrarca, V. Tucci, and M. Vitelli, "EM fields associated with lightning channels: On the effect of tortuosity and branching," *IEEE Trans. on Electromagnetic Compatibility*, Vol. 42, No. 4, 394–404, Nov. 2000.
27. Petrarca, C., "Geometrical and physical parameters affecting distant electric fields radiated by lightning return strokes," *Progress In Electromagnetics Research B*, Vol. 58, 167–180, 2014.
28. Chia, K. L. and A. C. Liew, "Effect of tortuosity of lightning stroke path on lightning electromagnetic fields," *Asia-Pacific Symposium on EMC*, 251–254, Singapore, 2008.
29. Song, T. X., Y. H. Liu, and J. M. Xiong, "Computations of electromagnetic fields radiated from complex lightning channels," *Progress In Electromagnetics Research*, Vol. 73, 93–105, 2007.
30. Meredith, S. L., S. K. Earles, I. N. Kostanic, N. E. Turner, and C. E. Otero, "How lightning tortuosity affects the electromagnetic fields by augmenting their effective distance," *Progress In Electromagnetics Research B*, Vol. 25, 155–169, 2010.
31. Andreotti, A., G. Lupo, and C. Petrarca, "Evaluation of EM fields from return stroke for indirect — Lightning protection of wind turbines," *2013 International Conference on Clean Electrical Power (ICCEP)*, 755–759, Alghero, Italy, Jun. 2013.
32. Idone, V. P. and R. E. Orville, "Channel tortuosity variation in Florida triggered lightning," *Geophysical Research Letters*, Vol. 15, No. 7, 645–648, Jul. 1988.
33. Jackson, J. D., *Classical Electrodynamics*, John Wiley & Sons, 1975.
34. Heidler, F., "Traveling current source model for LEMP calculation," *6th Int. Zurich Symposium on Electromagnetic Compatibility*, 157–162, Zurich, Switzerland, 1985.
35. Nucci, C. A., G. Diendorfer, M. A. Uman, F. Rachidi, M. Ianoz, and C. Mazzetti, "Lightning return stroke current models with specified channel-base current: A review and comparison," *Journal of Geophysical Research*, Vol. 95, No. D12, 20395–20408, Nov. 1990.
36. Rakov, V. A. and A. A. Dulzon, "A modified transmission line model for lightning return stroke field calculations," *9th Int. Symposium on Electromagn. Compat.*, 229–235, Zurich, Switzerland, Mar. 1991.
37. Baba, Y. and V. Rakov, "Electric and magnetic fields predicted by different electromagnetic models of the lightning return strokes versus measured fields," *IEEE Trans. on Electromagnetic Compatibility*, Vol. 51, No. 3, 479–487, Nov. 2009.
38. Lin, Y. T., M. A. Uman, J. A. Tiller, R. D. Brantley, W. H. Beasley, E. P. Krider, and C. D. Weidman, "Characterization of lightning return stroke electric and magnetic fields from simultaneous two-station measurements," *Journal of Geophysical Research*, Vol. 84, 6307–6314, 1979.
39. Jerauld, J., M. A. Uman, V. A. Rakov, K. J. Rambo, D. M. Jordan, and G. H. Schnetzer, "Electric and magnetic fields and field derivatives from lightning stepped leaders and first return strokes measured at distances from 100 to 1000 m," *Journal of Geophysical Research*, Vol. 113, No. D17111, 1–15, Sep. 2008.
40. Uman, M., V. Rakov, G. H. Schnetzer, K. J. Rambo, D. E. Crawford, and R. J. Fisher, "Time derivative of the electric field 10, 14 and 30 m from triggered lightning strokes," *Journal of Geophysical Research*, Vol. 105, No. D12, 15577–15595, 2000.
41. Rubinstein, M., F. Rachidi, M. A. Uman, R. Thottappillil, V. A. Rakov, and C. A. Nucci, "Characterization of vertical electric fields 500 m and 30 m from triggered lightning," *Journal of Geophysical Research*, Vol. 100, No. D5, 8863–8872, 1995.
42. Chen, M., Y. Du, and W. Dong, "Some new observations of lightning spectra in the bands above 25 MHz," *Radio Science Conference*, 635–637, Aug. 2004.
43. Le Vine, M., "Review of measurements of the RF spectrum of radiation from lightning," *Meteorology and Atmospheric Physics*, No. 37, 195–204, 1987.
44. Willett, J. C., J. C. Bailey, J. C. Leteinturier, and E. P. Krider, "Lightning electromagnetic radiation field spectra in the interval from 0.2 to 20 MHz," *Journal of Geophysical Research*, Vol. 95, No. 20, 367–387, 1990.